Int J Heat Mass Transfer Vol 33 No 11, pp 2503–2509, 1990
Printed in Great Britain

0017-9310/90 $3 00+0 00


# Structure of turbulent reacting gas jets in liquids at different temperatures and pressures

S. H CHAN and T. R SHEN

Department of Mechanical Engineering, University of Wisconsin–Milwaukee, P O. Box 784, Milwaukee, WI 53201, U S A

(*Received* 2 *August* 1989 *and in final form* 14 *December* 1989)

**Abstract**—New equilibrium state relationships have been constructed for the liquid metal combustion simulation reactants hydrogen chloride gas as oxidant and ammonia aqueous solution as fuel. The state relationships have been employed to predict the structure of sonic, turbulent, reacting HCl gas jets submerged in ammonia aqueous solutions. Fuel temperature and ambient pressure effects have been examined It is found that either raising fuel temperature or lowering ambient pressure will increase the fuel evaporation, decrease the entrainment rate, delay the completion of reaction and extend greatly the total jet penetration length Good agreement has been found with reported experimental data of the jet penetration length over a wide range of experimental conditions with varying fuel concentration, temperature and ambient pressure

## 1. INTRODUCTION

THE STORED chemical energy propulsion systems use alkali metals as fuel and halogen or halogenated gases as oxidant [1] In these power systems, thermal energy is produced in a combustor filled with a molten metal fuel, into which a choked submerged jet of reacting gas oxidant is injected. The reaction forms a complex, multiphase, turbulent diffusion flame. The combustor is unique in that power density is high and combustion products are condensable so that all products are containable in the reactant vessel itself. Thus no discharge of products is necessary during operation and the propulsion system is unaffected by the surrounding back pressure, making it well suited for underwater applications

In our prior theoretical study [2], two parts were proposed for the analysis of liquid metal combustion First a formulation and code development for chemical equilibrium computations of general multiphase reacting systems were proposed. The reactants in the system can be ideal, non-ideal, electrolytic or non-electrolytic mixtures The second part constitutes physical models for the prediction of the turbulent structure of the liquid metal diffusion flame. The first part is for the construction of equilibrium state relationships which are prerequisite information necessary for flow computation in the second part. Applications were made to predict the reaction of a gaseous hydrogen chloride (oxidant) jet submerged in an ammonia aqueous solution (fuel), when limited experimental data was available for comparison [3] Since then, much more extensive experimental data have been reported over a wide range of system pressure and fuel temperature conditions [4]. The objective of the present study is to continue our prior study to examine the pressure and temperature effects on turbulent structure of such diffusion reacting jets This, together with the prior study which focused on fuel concentration effects, constitutes a better verification of the theoretical work proposed previously [2]

It is noted that the reaction of HCl gas/$NH_3$ aqueous solution simulates well many characteristics of liquid metal combustion—multiphase, exothermic reaction, fuel vaporization, condensation of products and excess reactants [3] In fact analysis of HCl gas/$NH_3$ solution reaction is by no means simpler than liquid metal reaction since the former also involves an additional process, namely, dissolution of HCl gas in ammonia solution, which is not found in liquid metal combustion Therefore, successful prediction of HCl/$NH_3$ reaction will lend further support to the analytical work proposed previously for liquid metal combustion

## 2. ANALYSIS

Details of the theoretical model and formulation have been described previously [2] They are briefly summarized below.

The method of calculation of chemical equilibrium was based on the principle of minimization of Gibbs free energy subject to the constraints the conservation of elements and balance of charges. The latter is needed since ions are present in electrolyte solutions With the introduction of proper partial molal (or molar) enthalpy and chemical potential expressions for imperfect gases, solutes and solvent of non-ideal and electrolytic solutions, as well as proper activity coefficient expressions and thermodynamic data, the system of non-linear equations is solved by a modified Newton–Raphson iteration scheme.

## NOMENCLATURE

| | |
|---|---|
| $a$ | gravitational acceleration [m s$^{-2}$] |
| $D$ | injector diameter [m] |
| $d$ | jet diameter at the end of the expansion region [m] |
| $f$ | mixture fraction |
| $g$ | square of the mixture fraction fluctuations |
| $k$ | turbulent kinetic energy [J kg$^{-1}$] |
| $P$ | probability density function |
| $r$ | radial distance from axis of symmetry [m] |
| $S_\phi$ | source term in governing equations |
| $T$ | temperature [K] |
| $u$ | axial velocity [m s$^{-1}$] |
| $v$ | radial velocity [m s$^{-1}$] |
| $x$ | axial distance [m] |
| $Y_i$ | mass fraction of species $i$ |

Greek symbols

| | |
|---|---|
| $\alpha$ | void fraction |
| $\gamma_i$ | activity coefficient of species $i$ |
| $\varepsilon$ | dissipation rate of turbulent kinetic energy [J kg$^{-1}$ s$^{-1}$] |
| $\mu$ | molecular viscosity [kg m$^{-1}$ s$^{-1}$] |
| $\mu_{\text{eff}_\phi}$ | effective viscosity [kg m$^{-1}$ s$^{-1}$] |
| $\mu_t$ | turbulent viscosity [kg m$^{-1}$ s$^{-1}$] |
| $\rho$ | density [kg m$^{-3}$] |
| $\sigma$ | turbulent Schmidt or Prandtl number |

Subscripts

| | |
|---|---|
| aq | aqueous solution |
| c | crystal |
| g | vapor phase |
| l | liquid phase |
| 0 | injector exit condition |
| $\infty$ | ambient condition |

Superscripts

| | |
|---|---|
| | time averaged quantity |
| ~ | mass averaged quantity |

Like the last paper, the equilibrium code developed is now applied to the reacting pair of gaseous HCl as oxidant and aqueous $NH_3$ solutions as fuel. The possible species considered in the liquid phase after reaction are: $H^+$, $NH_4^+$, $Cl^-$, $NH_{3(aq)}$ and $H_2O_{(l)}$. The gas phase species allowed are $H_2O_{(g)}$, $NH_{3(g)}$ and $HCl_{(g)}$, while $NH_4Cl_{(c)}$ crystal is the one considered in the solid phase. Chemical equilibrium composition and thermodynamic properties after mixing for ten representative experimental conditions will be constructed later. Those conditions before mixing [3] are summarized in Table 1, which lists the concentration of ammonia fuel in aqueous solution ($Y_{NH_3,\infty}$), the solution (ambient bath) temperature ($T_\infty$) and the ambient bath pressure ($P_\infty$). In all test runs, the choked HCl gas jets are discharged vertically through the bottom of ammonia aqueous solution through a nozzle diameter of 1 mm (i.e. $D = 1$ mm). The HCl gas was supplied by a constant source with a stagnation pressure of 0.377 MPa (40 psia) and a stagnation temperature of 293.15 K.

The primary variable in the first group (cases A–E) is the ammonia concentration in aqueous solution (i.e. fuel concentration variation). Its effects were studied in the last paper. Fuel bath temperature and system pressure are the variables in the second (cases E–H) and third (cases I and J) group, respectively. Their effects are the subject of present interest.

The computation of reaction zone structure of turbulent HCl gas jets submerged in aqueous ammonia solution uses the model and the method described in the previous paper [2], which follows closely the method developed by Lockwood and Naguib [5] and Chen and Faeth [6], etc. The method uses the locally homogeneous flow approximation for multiphase flow, the conserved scalar method for mass transfer

Table 1. Experimental conditions and comparison of theoretical and experimental results

| Case No | $NH_{3(aq)}$ | | | HCl initial conditions | | | | Plume length ($x/D$) results | | |
|---|---|---|---|---|---|---|---|---|---|---|
| | | | | | | | | Experimental | | Theoretical |
| | $Y_{NH_3,\infty}$ (%) | $T_\infty$ (°C) | $P_\infty$ (kPa) | $T_0$ (°C) | $\rho_0$ (kg m$^{-3}$) | $\bar{u}_0$ (m s$^{-1}$) | $d \times 10^3$ (m) | Range | Mean | Mean |
| A | 0 | 20 | 101.3 | −72.15 | 2.208 | 382.2 | 1.087 | 3–4.5 | 3.9 | 3.8 |
| B | 10.6 | 20 | 101.3 | −72.15 | 2.208 | 382.2 | 1.087 | 8–13 | 11.3 | 9.9 |
| C | 19 | 20 | 101.3 | −72.15 | 2.208 | 382.2 | 1.087 | 12–22 | 17.3 | 20 |
| D | 25.6 | 20 | 101.3 | −72.15 | 2.208 | 382.2 | 1.087 | 30–48 | 43 | 45 |
| E | 12 | 14 | 101.3 | −72.15 | 2.208 | 382.2 | 1.087 | 5–11 | 7.5 | 9.5 |
| F | 12 | 45 | 101.3 | −72.15 | 2.208 | 382.2 | 1.087 | 12–24 | 20.4 | 26 |
| G | 11.9 | 50 | 101.3 | −72.15 | 2.208 | 382.2 | 1.087 | 24–37 | 31.4 | 37.7 |
| H | 11.9 | 59.5 | 101.3 | −72.15 | 2.208 | 382.2 | 1.087 | 57–73 | 63.9 | 85.0 |
| I | 12 | 25 | 50.5 | −108.11 | 1.342 | 452 | 1.283 | 22–32 | 27.1 | 23.0 |
| J | 12 | 25 | 84.4 | −82.05 | 1.937 | 403.3 | 1.13 | 9–20 | 15.9 | 13.3 |

and the $K$–$\varepsilon$–$g$ model for turbulence The transport equations solved are summarized in ref [2] and will not be repeated here Basically they include the Favre-averaged, parabolic forms of continuity, momentum, mixture fraction ($\tilde{f}$), turbulence kinetic energy ($k$), dissipation rate of turbulent kinetic energy ($\varepsilon$) and the square of the mixture fraction fluctuations ($g$) Other mean scalar properties not solved by the transport equations are determined by the equilibrium state relationship weighted by a clipped Gaussian profile of probability density function The latter is governed by two parameters, the variance and the most probable value, both of which are in turn determined by $\tilde{f}$ and $g$ solved at each local point in the flow More details can be found in ref [2]

## 3 NUMERICAL COMPUTATIONS AND THEORETICAL RESULTS

The equilibrium states achieved after reaction have been calculated as a function of mixture fraction $f$ for experimental conditions listed in Table 1 The mixture fraction is so defined that $f = 1$ designates the pure HCl gas at the end condition of the expansion region (see later) while $f = 0$ designates pure aqueous ammonia solution at bath conditions Two representative cases, E and H, are presented in Figs 1 and 2, respectively, to show effects of initial fuel temperature on equilibrium state relationships In each set of figures, the equilibrium mixture void fraction, mass fractions of liquid, vapor and solid phases, mixture temperature and density are presented in part (a), such as Fig 1(a) The detailed mass fractions of all individual species, including electrolytes, are given in part (b), like Fig 1(b). Similarly, for pressure effects, the equilibrium state relationships for cases I and J are shown in Figs. 3 and 4, respectively

Once the equilibrium state relationships have been constructed, the structure of the reacting HCl gas jets submerged in $NH_3$ aqueous solutions can be readily

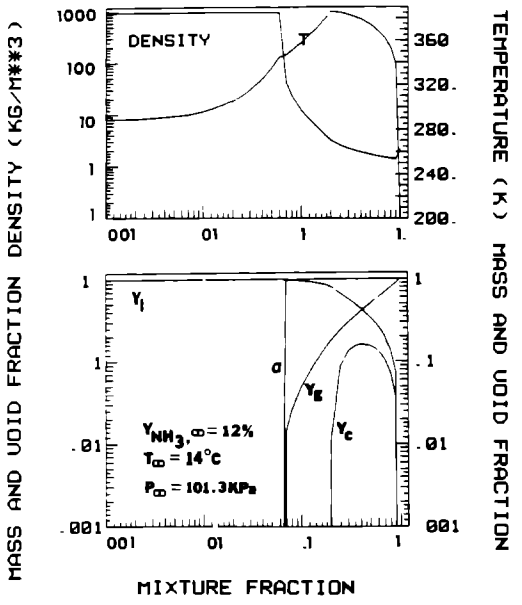


FIG 1(a) Equation of state (density, temperature, void fraction and mass fractions) for HCl–$NH_3$–$H_2O$ system at $Y_{NH_3,\infty}$ = 12%, $T_\infty$ = 14 C and $P_\infty$ = 101 3 kPa (case E)

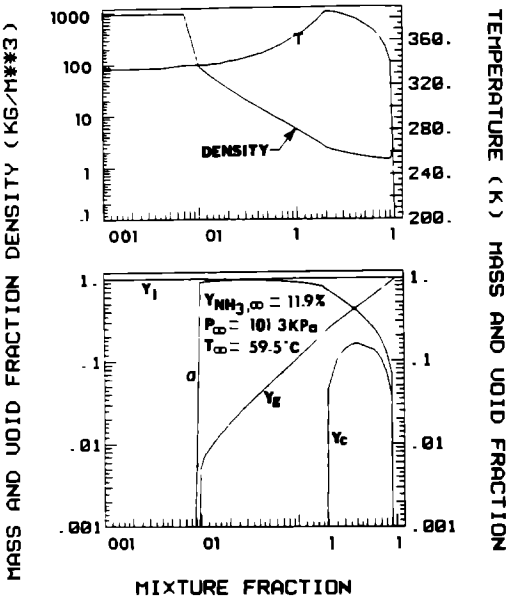


FIG 2(a) Equation of state (density, temperature, void fraction and mass fractions) for HCl–$NH_3$–$H_2O$ system at $Y_{NH_3,\infty}$ = 11 9%, $T_\infty$ = 59 5°C and $P_\infty$ = 101 3 kPa (case H)

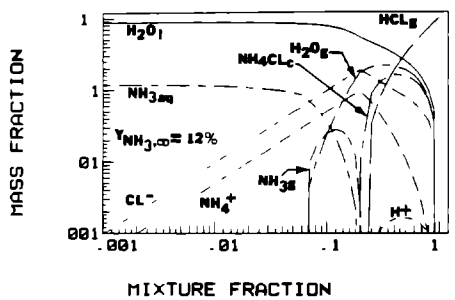


FIG 1(b) Equilibrium composition of HCl–$NH_3$–$H_2O$ system at $Y_{NH_3,\infty}$ = 12%, $T_\infty$ = 14°C and $P_\infty$ = 101 3 kPa (case E)

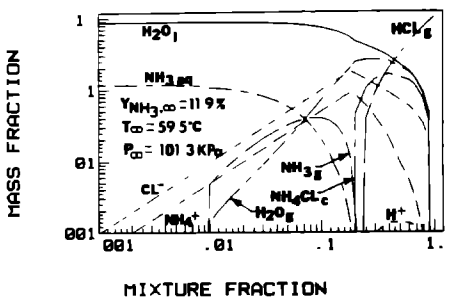


FIG 2(b) Equilibrium composition of HCl–$NH_3$–$H_2O$ system at $Y_{NH_3,\infty}$ = 11 9%, $T_\infty$ = 59 5°C and $P_\infty$ = 101 3 kPa (case H)

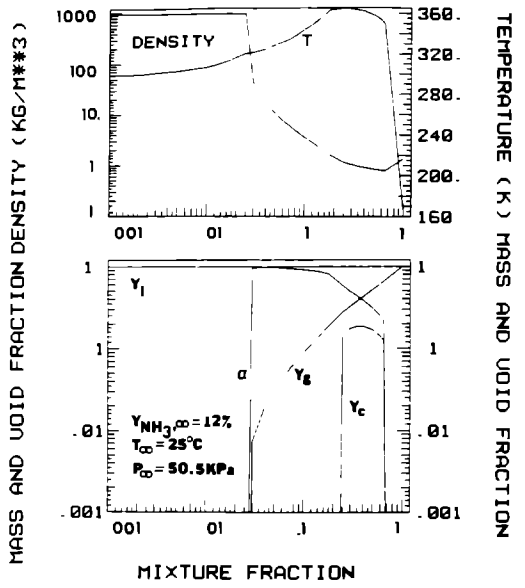


FIG 3(a) Equation of state (density, temperature, void fraction and mass fractions) for HCl–$NH_3$–$H_2O$ system at $Y_{NH_3,\infty}$ = 12%, $T_\infty$ = 25 C and $P_\infty$ = 50 5 kPa (case I)

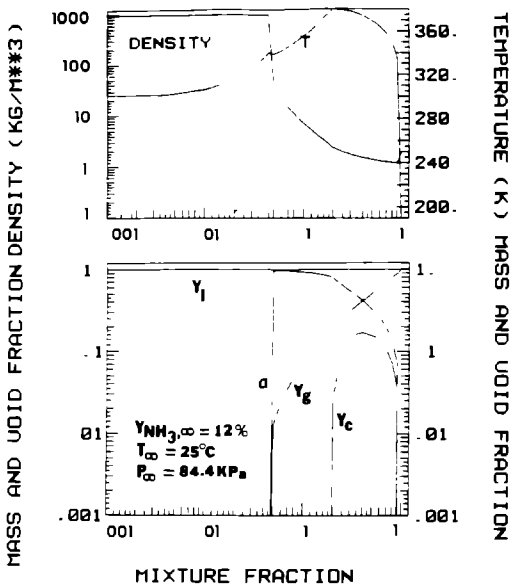


FIG 4(a) Equation of state (density, temperature, void fraction and mass fractions) for HCl–$NH_3$–$H_2O$ system at $Y_{NH_3,\infty}$ = 12%, $T_\infty$ = 25 C and $P_\infty$ = 84 4 kPa (case J)

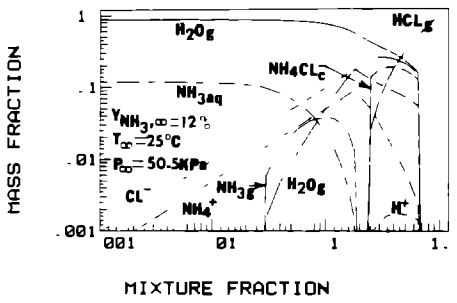


FIG 3(b) Equilibrium composition of HCl–$NH_3$–$H_2O$ system at $Y_{NH_3,\infty}$ = 12%, $T_\infty$ = 25 C and $P_\infty$ = 50 5 kPa (case I)

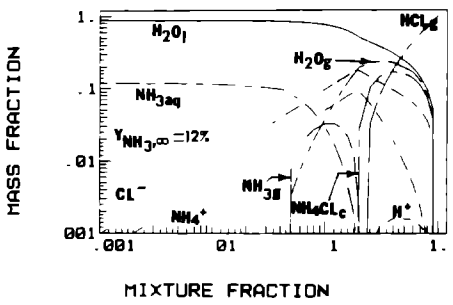


FIG 4(b) Equilibrium composition of HCl–$NH_3$–$H_2O$ system at $Y_{NH_3,\infty}$ = 12%, $T_\infty$ = 25 C and $P_\infty$ = 84 4 kPa (case J)

computed using the flow model summarized above To account for underexpansion effects, the sonic jets discharged from the nozzle are assumed to immediately expand isentropically to the ambient pressure of the solutions By mass and energy balances, the jet's temperature, density, velocity and diameter at the end of the underexpansion region have been calculated and listed in Table 1 Those end conditions are found to satisfy the conservation of momentum within 2.6–10 6% They serve as the initial conditions of computation The underexpansion length is neglected as compared to the plume length The calculating domain was started at the end of the expansion region using the values of velocity, density, and jet radius calculated above Since exact initial values, such as $k_0$ and $\varepsilon_0$, were not available, they had to be estimated in a manner similar to the previous studies [2] All initial conditions were assumed to be uniform across the entire jet and were specified Due to symmetry, the radial gradients of $\tilde{u}$, $\tilde{f}$, $k$, $\varepsilon$ and $g$ at the plume axis were set to zero At the outer free boundary, $g$ was simply set to zero, very small values of $\tilde{u}$ and $\tilde{f}$ (0 005$\tilde{u}_0$ and 0 0005$\tilde{f}_0$, respectively) were assumed, while $k$ and $\varepsilon$ were estimated in terms of $\tilde{u}$ by $k_0 = (0\ 03\tilde{u})^2$ and $\varepsilon_0 = (0\ 03u)^3/d$ At later steps, $k$ and $\varepsilon$ at the free stream boundary were obtained by solving the governing equations with the convective and diffusive terms neglected as follows

$$k_d = k_u - \varepsilon/\tilde{u} \cdot Dx$$

$$\varepsilon_d = \varepsilon_u - C_\varepsilon \varepsilon_u^2 \cdot Dx/(k\tilde{u})$$

where subscripts d and u denote downstream and upstream, respectively, and $Dx$ is the forward-step size in the x-direction in meters The rest of the computational details are given in the previous study [2].

Figures 5 and 8 present respectively the predicted mean transport values along the centerline axis of vertical HCl gas jets injected into the ammonia solu-

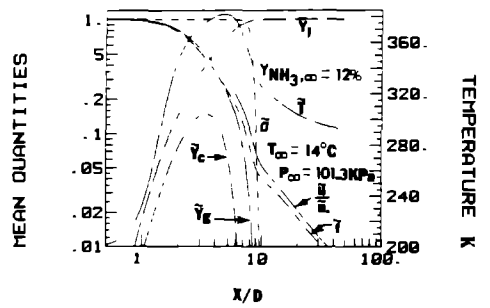


FIG 5 Predicted mean properties along the jet axis at $Y_{NH_3,\infty}$ = 12%, $T_\infty$ = 14°C and $P_\infty$ = 101.3 kPa (case E)

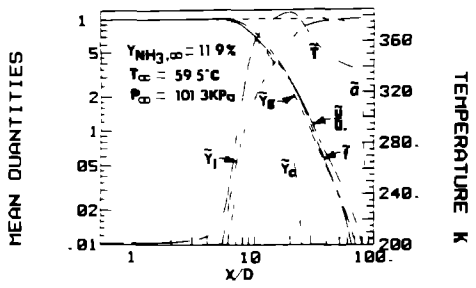


FIG 8 Predicted mean properties along the jet axis at $Y_{NH_3,\infty}$ = 11.9%, $T_\infty$ = 59.5 C and $P_\infty$ = 101.3 kPa (case H)

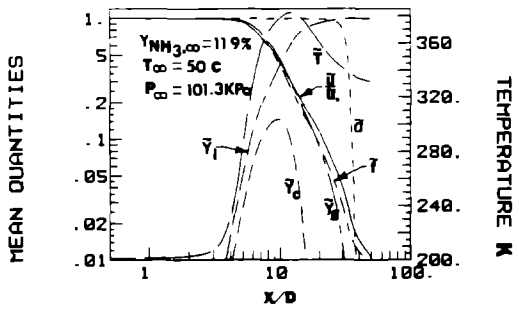


FIG 6 Predicted mean properties along the jet axis at $Y_{NH_3,\infty}$ = 12%, $T_\infty$ = 45°C and $P_\infty$ = 101.3 kPa (case F)

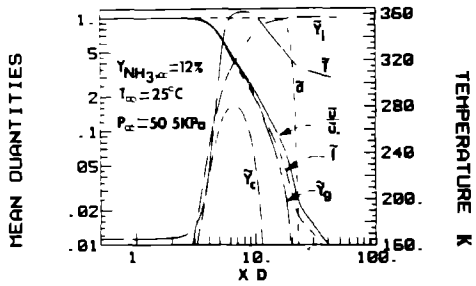


FIG 9 Predicted mean properties along the jet axis at $Y_{NH_3,\infty}$ = 12%, $T_\infty$ = 25°C and $P_\infty$ = 50.5 kPa (case I)

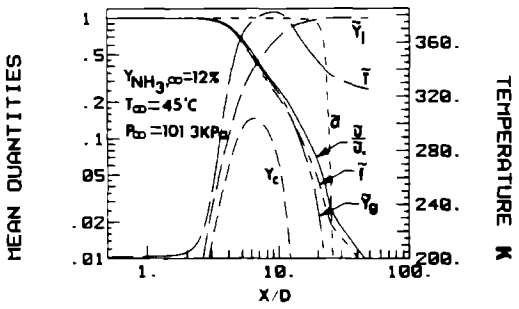


FIG 7 Predicted mean properties along the jet axis at $Y_{NH_3,\infty}$ = 11.9%, $T_\infty$ = 50°C and $P_\infty$ = 101.3 kPa (case G)

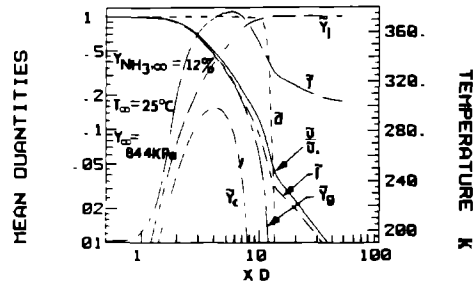


FIG 10 Predicted mean properties along the jet axis at $Y_{NH_3,\infty}$ = 12%, $T_\infty$ = 25°C and $P_\infty$ = 84.4 kPa (case J)

tion pool for experimental conditions of cases E–H They include the mean centerline velocity ($\tilde{u}/\tilde{u}_0$), mixture fraction ($\tilde{f}$), temperature ($\tilde{T}$), void fraction ($\tilde{\alpha}$) and mass fractions of gas ($\tilde{Y}_g$), liquid ($\tilde{Y}_l$) and solid ($\tilde{Y}_c$) phases. For cases I and J, they are shown in Figs. 9 and 10, respectively

To assess bath temperature effects, the species mass fraction profiles of cases E and H shown in Figs. 1(b) and 2(b) are examined and compared first The fuel temperature has the most significant effect on fuel vapor, namely ammonia and water vapors. As temperature increases from 14 to 59 5°C, the span of the excess $NH_{3(g)}$ region is greatly extended from $f$ = 0 2 to a lower value of mixture fraction, namely from $f$ = 0 2–0.07 to 0 2–0 01. Similarly, the water vapor range is extended from $f$ = 1–0.07 to 1–0.01 The combined effect of $NH_{3(g)}$, $H_2O_{(g)}$ and the oxidant $HCl_{(g)}$ can be examined by comparing Figs. 1(a) and 2(a) It is seen that the gas phase mass fraction and the mixture void fraction have accordingly been extended from $f$ = 1–0 07 to 1–0.01 when the bath temperature increases from 14 to 59.5°C

The extension of the scalar property range in these state relationship figures (Figs. 1 and 2) should stretch those scalar property profiles in the flow structure diagram (Figs 5 and 8) further downstream. This is obvious if one notices that the scalar properties near the nozzle exit correspond roughly to those given in the state relationships when $f$ is close to 1. As one travels downstream, the scalar properties in the flow structure diagram correlate with those in the state relationship diagram with decreasing values of $f$ Therefore, when bath temperature increases, equilibrium fuel vapor and void fraction appear at lower values of $f$, causing a significant change in jet structure

and substantial elongation of total penetration length as shown in Figs 5 and 8 The calculated penetration lengths, which are arbitrarily taken as the length where void fraction reduces to 0 01, are also listed in Table 1 for ease of comparison

The above elongation of the total penetration length is predominantly an effect due to lower subcooling of the liquid bath, the flow with lower subcooling needs to take a longer distance to reach the "cut-off" condition Another interesting phenomenon we noticed from the detailed printouts of the computations is that vaporization in the jet significantly affects the entrainment rate, namely, higher fuel temperatures trigger more evaporation but less entrainment rate of the ambient fuel Comparing the two cases in Figs 5 and 8, the one with the higher temperature clearly shows higher values of $\tilde{Y}_g$ and $\tilde{f}$ Higher $\tilde{Y}_g$ values mean larger mass fraction attributed to the gaseous phase due to more evaporation, and higher $f$ values imply less entrainment in view of the definition of the mixture fraction Physically what happens is as follows Since $NH_3$ vapor is lighter than the ambient aqueous solution and HCl gas in the main jet stream, as more $NH_3$ evaporates from the jet interphase boundary, the jet mixture density reduces near the boundary. Consequently the turbulent viscosity and the entrainment rate of the ambient fuel should reduce accordingly [7] The resulting $\tilde{f}$ and $\tilde{u}/\tilde{u}_0$ profiles along the jet axis should then decrease at a rate slower for case H (Fig 8) with higher ambient temperature. They in turn prolong the void fraction profile and delay appearance of liquid ($\tilde{Y}_l$) and crystal ($\tilde{Y}_c$) mass fraction profiles to axial locations of larger $x/D$ values Therefore, by referring to Figs 5 and 8, when $T_\infty$ increases from 14 to 59.5°C, the plume penetration length increases by an order of magnitude because of the entrainment and subcooling effects

As to pressure effects, let us examine case I ($P_\infty$ = 50 5 kPa) and case J ($P_\infty$ = 84 4 kPa) Their state relationships are compared in Figs 3 and 4 and their flow structures in Figs 9 and 10 The comparison shows that, like temperature effects, lower ambient pressure produces larger spans of $NH_3$ and $H_2O$ vapor regions in state relationship diagrams and prolongs $\tilde{f}$ and $\tilde{x}$ profiles in flow structure diagrams. In fact, either lowering pressure or raising temperature yields the same net effect, namely, reducing subcooling of fuel Thus the above discussion about temperature effects is equally applicable here which does not need to be reiterated

## 4 COMPARISON WITH EXPERIMENTAL DATA

All the calculated reacting jet penetration lengths are summarized and compared to the experimental data [4] as shown in Table 1 The total penetration lengths were found experimentally to be oscillating in nature, and both their ranges of oscillation and their mean values are listed in the table The comparison shows that the calculated results somewhat overpredict the mean penetration length in cases E–H but slightly underpredict cases I and J Nevertheless, most of them, including cases A–D, are within the oscillating range of the plume length The relatively large oscillation is not attributed to experimental error but rather is the unique nature observed in the reacting system [4] It has at least been partially accounted for in the present study by the use of the probability density function approach The comparison of ten cases indicated in the table is considered to be rather extensive since variation of experimental conditions in fuel concentration, fuel temperature and ambient pressure have been covered in cases A–E, E–H and I–J, respectively In addition, reaction of turbulent submerged HCl gas jets in ammonia solutions is in reality rather complex It involves a dissolution process (HCl gas dissolving in aqueous solution) not found in metal combustion, and many processes found in liquid metal combustion, including heat of reaction, evaporation, condensation and solubility effects Thermal radiation and immiscibility effects which may be important in liquid metal combustion are however not important in the HCl–$NH_3$ system Separate effort is under way to model thermal radiation/turbulence interaction for future liquid metal combustion computation The immiscibility effect can be satisfactorily accounted for by the present model which will be reported later The satisfactory agreement in all cases of computations of the $HCl_{(g)}/NH_{3(aq)}$ reaction seems to attest the validity of the theoretical work proposed for the liquid metal combustion, at least for the realistic modeling of the global characteristics of the flow structure

Finally, an attempt is made to see if the current numerical predictions of total penetration length can be correlated by a simple equation Following the work of Cho *et al* [4], the calculated plume lengths are correlated by

$$L/D = C\frac{\Delta H_r}{C_p \Delta T}\left(\frac{\rho_0}{\rho_\infty}\right)^{1/2}$$

where $\Delta H_r$ is the heat of reaction per unit mass of oxidant (J $g^{-1}$ of HCl), $C_p$ the specific heat of bath liquid (J $°C^{-1}$ $g^{-1}$ of ammonia solution) and $\Delta T$ the degree of subcooling (saturation temperature of ammonia vapor corresponding to the bath pressure and ammonia concentration in solution minus the bath temperature) in K By the least square method, the correlation constant is found to be 16 48 The absolute percentage difference between the predicted values and those from the correlation is within 23%

## 5 CONCLUSIONS

New equilibrium state relationships for the reactants of gaseous hydrogen chloride and aqueous ammonia solution have been constructed They have been used to study the effects of fuel temperature and ambient pressure on the structure of turbulent,

diffusion, reacting HCl jets in ammonia aqueous solutions It is found that raising the fuel temperature or lowering the ambient pressure will increase vaporization of fuel liquid to the jet, reduce the entrainment flux of the liquid, delay the completion of reaction and greatly extend the total jet penetration length. Satisfactory agreement with extensive experimental data lends further support to the validity of our prior theoretical work proposed for the equilibrium computation of general multiphase reacting systems and for modeling the structure of turbulent, diffusion jets in reacting liquids

*Acknowledgements*—This research was sponsored by the Office of Naval Research, Contract No N00014-85-K-0752 and N00014-89-J-1267, under the technical management of Drs G Roy, R S Miller and L Parnell

## REFERENCES

1 T G Hughes, R B Smith and D H Kiley, Stored chemical energy propulsion system for underwater applications, *J Energy* **7**, 128–133 (1983)

2 S H Chan, P J Janke and T R Shen, Equilibrium computations of multiphase nonideal electrolytic systems and structure of turbulent reacting dissolving jets, *The Twenty-second Symp (Int) on Combustion*, pp 721–729 (1988)

3 D H Cho, D R Armstrong and L Bova, Dynamic behavior of reacting gas jets submerged in liquids Presented at the National Heat Transfer Conf, Pittsburgh, Pennsylvania, Paper No 87-HT-67, 9–12 August (1987)

4 D H Cho D R Armstrong and L Bova, Heat release effects of reacting gas jets in liquids, *ASME Proc 1988 National Heat Transfer Conf* (Edited by H R Jacobs), Vol 1, pp 27–34 (1988) Also in *Chem Engng Sci* **45**, 423–435 (1990)

5 F C Lockwood and A S Naguib, The prediction of the fluctuations in the properties of free, round-jet, turbulent, diffusion flames, *Combust Flame* **24**, 109–124 (1975)

6 L D Chen and G M Faeth, Structure of turbulent reacting gas jets submerged in liquid metals, *Combust Sci Technol* **11**, 111–131 (1983)

7 D B Spalding, *GENMIX A General Computer Program for Two-dimensional Parabolic Phenomena* Pergamon Press, Oxford (1977)

## STRUCTURE DE JETS TURBULENTS GAZEUX EN REACTION DANS DES LIQUIDES A DIFFERENTES TEMPERATURES ET PRESSIONS

**Résumé**—De nouvelles relations d'état d'équilibre sont établies pour la simulation de la combustion de métal liquide le chlorure d'hydrogène gazeux comme oxydant et une solution aqueuse d'ammoniac comme combustible. Ces relations ont été employées pour prédire la structure des jets gazeux soniques, turbulents de HCl submergés dans l'ammoniaque Les effets de la température du combustible et de la pression ambiante sont étudiés Un accroissement de la température, ou une diminution de la pression, accroit l'évaporation du combustible, diminue le taux d'entrainement, retarde la réaction et augmente la longueur totale de pénétration du jet. Un bon accord est trouvé avec les données expérimentales connues sur la longueur de pénétration du jet, dans un large domaine du conditions expérimentales avec différentes concentrations de combustible, différentes températures et plusieurs pressions ambiantes

## DIE STRUKTUR TURBULENTER REAGIERENDER GASSTRAHLEN IN FLÜSSIGKEIT BEI UNTERSCHIEDLICHEN TEMPERATUREN UND DRÜCKEN

**Zusammenfassung**—Für die folgenden Reaktanden, welche die Verbrennung von Flüssigmetallen simulieren sollen, werden neue Gleichgewichtsbeziehungen aufgestellt Wasserstoffchloridgas als Oxydant und eine wäßrige Ammoniaklosung als Brennstoff Die Zustandsbeziehungen werden für die Berechnung der Struktur von schallnahen turbulenten reagierenden HCl-Gasstrahlen in waßrigen Ammoniaklösungen verwendet Es werden die Einflusse der Brennstofftemperatur und des Umgebungsdrucks untersucht Dabei ergibt sich, daß sowohl ein Ansteigen der Brennstofftemperatur wie auch ein Absinken des Umgebungsdrucks die Brennstoffverdampfung beschleunigt, das Entrainment verringert, den Abschluß der Reaktion verzogert und die gesamte Eindringlange des Strahls wesentlich vergroßert Für die Eindringlänge des Strahls ergibt sich gute Übereinstimmung mit vorhandenen Versuchsdaten, und zwar in einem weiten Bereich der Versuchsbedingungen bei veränderlichen Werten der Brennstoffkonzentration, der Temperatur und des Umgebungsdrucks

## СТРУКТУРА ТУРБУЛЕНТНЫХ РЕАГИРУЮЩИХ ГАЗОВЫХ СТРУЙ В ЖИДКОСТЯХ ПРИ РАЗЛИЧНЫХ ТЕМПЕРАТУРАХ И ДАВЛЕНИЯХ

**Аннотация**—Получены новые зависимости, описывающие равновесное состояние реагентов в модели горения жидких металлов: газообразного хлористого водорода в качестве окислителя и водного раствора аммиака в качестве топлива Уравнения состояния использовались для определения структуры турбулентных реагирующих газовых струй HCl, текущих со звуковой скоростью в водных растворах аммиака. Исследованы эффекты температуры топлива и давления окружающей среды. Найдено, что увеличение температуры топлива или уменьшение давления окружающей среды приводит к усилению испарения топлива, снижению скорости уноса, запаздыванию завершения реакции и значительно увеличивает общую длину проникновения струи. Обнаружено хорошее соответствие между полученными результатами и имеющимися в литературе экспериментальными данными по длине проникновения струи в широком диапазоне условий опытов с изменяющимися концентрацией и температурой топлива, а также давлением окружаюрей среды.